typeset using JPSJ.sty <ver.1.0b>

Effect of Hydrostatic Pressure on the Low-Temperature Phase Transitions in Rb_2ZnBr_4

Hirotake SHIGEMATSU, Masato KUBOTA[1], Masakazu NISHI[1], Hiroyuki MASHIYAMA[2] and Tuneo MATSUI

Department of Quantum Engineering, Graduate School of Engineering, Nagoya University, Nagoya 464-8603
[1]*Neutron Scattering Laboratory, I. S. S. P., University of Tokyo, Tokai, Ibaraki 319-1106*
[2]*Department of Physics, Faculty of Science, Yamaguchi University, Yamaguchi 753-8512*

(Received February 26, 1999)

The effect of hydrostatic pressure on the low-temperature structural phase transitions in Rb_2ZnBr_4 has been investigated by the use of neutron scattering technique. The phase III-to-IV transition temperature, T_3=112 K at atmospheric pressure, increases with applying pressure with a rate of 7 K/kbar. The phase IV-to-V transition temperature, T_4=76 K at atmospheric pressure, decreases with applying pressure with a rate of -45 K/kbar. At high pressure, two high-order pseudo-commensurate phases characterized by wave vectors $q_z \simeq \frac{3}{11}$ and $\frac{4}{15}$ are observed in addition to the already known commensurate ones of $q_z=\frac{2}{7}$ and $\frac{1}{4}$. The space group of the commensurate phase of $q_z=\frac{1}{4}$ under high pressure is suggested to be $P2_1/c11$ from the extinction rule.

KEYWORDS: Rb_2ZnBr_4, structural phase transition, neutron scattering, hydrostatic pressure

§1. Introduction

Rubidium tetrabromozincate, Rb_2ZnBr_4, belongs to a family of crystals such as Rb_2ZnCl_4 with the β-K_2SO_4 type structure. Four phase transitions occur at temperatures T_i=347 K, T_C=187 K, T_3=112 K and T_4=76 K at atmospheric pressure. The five phases are summarized as follows: phase I ($T>T_i$, $Pmcn$, Z=4; a_0, b_0, c_0), phase II ($T_i>T>T_C$, incommensurate; a_0, b_0, $\sim 3c_0$), phase III ($T_C > T > T_3$, $P2_1cn$, Z=12, ferroelectricity//a; a_0, b_0, $3c_0$), phase IV ($T_3 > T > T_4$, ferroelectricity//a, antiferroelectricity//b; $2a_0$, $2b_0$, $3c_0$) and phase V ($T < T_4$, ferroelectricity//a, ferroelectricity//c, $C1c1$, Z=48; $2a_0$, $2b_0$, $3c_0$), where a_0, b_0 and c_0 are unit cell parameters in phase I.[1–6)]

Many of the A_2BX_4-type ferroelectrics, for example, Rb_2ZnCl_4, K_2ZnCl_4 and K_2CoCl_4, undergo the phase transition from ferroelectric phase III to monoclinic phase V ($C1c1$, Z=48), directly. On the other hand, in Rb_2ZnBr_4, there is another intermediate phase (phase IV), whose crystal

structure has not been determined as yet. In phase IV, there is an extra extinction rule that cannot be explained by space group symmetry.

We have presented four twin-structural models from the extinction rule, the extended space-group analysis, the spontaneous polarization, and so on.[7,8] The reflection intensities of eight structure factors $|F(\pm h \pm k \pm l)|^2$ in phase IV have the same magnitude, if the domain ratio is 1:1 in the twined structure. When the domain ratio deviates from 1:1, the intensity should not satisfy the mmm symmetry, if the space group belongs to the monoclinic one. In order to decide the space group of phase IV, we have to change the twin ratio by external parameters. Study of pressure effect on the phase transitions in Rb_2ZnBr_4 will provide useful information with respect both to the mechanism of the transitions at T_3 and T_4 and to the structures of phase IV and V.

The pressure-temperature phase diagram above T_3 has been investigated by neutron diffraction,[9,10] dielectric,[11,12] NQR[13,14] and elastic and birefringent[15] measurements. It has been reported that three commensurate phases of q_z=$\frac{2}{7}$, $\frac{1}{4}$ and 0, and several pseudo-commensurate phases of $q_z \simeq \frac{3}{10}$, $\frac{7}{24}$, $\frac{5}{17}$ and so on exist at high pressure. In this paper we will report the effect of hydrostatic pressure on the low-temperature phase transitions in Rb_2ZnBr_4 by means of neutron scattering.

§2. Experimental

Single crystals of Rb_2ZnBr_4 were grown by slow evaporation method from a saturated aqueous solution of RbBr and $ZnBr_2$ in the molar ratio 1:1 at 308 K.[8] About three months were needed to grow the single crystals more than 1cc in volume. The obtained crystals were colorless and transparent and showed poor cleavage perpendicular to the b-axis. Samples were annealed at 393 K for ten hours before an experiment in an air to avoid an influence of water contamination.

Triple-axis spectrometers C1-1 and 4G, installed in the guide hall and in the reactor hall, respectively, at JRR-3M reactor of the Japan Atomic Energy Research Institute (JAERI), Tokai, were used for neutron scattering. By the use of the C1-1 spectrometer, energy scans were done with a fixed incident neutron beam of $k_{\rm i}$=1.55 Å^{-1} with a pyrolytic graphite, PG002 monochromator and a PG002 analyzer for requiring a high energy resolution. A beryllium filter was used in order to cut off higher order reflections. Beam collimation of open-open-80'-80' was employed for inelastic scattering. The integrated intensities of Bragg and superlattice reflections were measured by using the double axis mode with open-open-80' collimation. In the 4G spectrometer, a fixed incident neutron beam of $k_{\rm i}$=2.57 Å^{-1} was used for measuring a little more high-angle reflections. The used conditions were the following: PG002 monochromator and 40'-40'-40' collimation.

In the both spectrometers, single crystals were cut to about 10 mm high and 5 mm in diameter, and the crystallographic [010] or [001] axis was parallel to the rod axis. Each rod sample was mounted in an Al micro-cell with a piece of NaCl crystal as pressure standard. The micro cell was placed inside a barrel-shaped cylinder made of ZrO_2, and was loaded in a clamp-type high-

pressure cell.[16] Pressure was applied at room temperature using Fluorinert: FC-75, as the pressure-transmitting fluid. The pressure was measured by monitoring the change of the lattice constant of NaCl and its uncertainty was within ± 0.05 kbar. On cooling from room temperature down to around 20 K, the pressure reduced above 60 %. However, it recovered reversibly on heating.

The sample temperature was controlled within 0.1 K by a TEMCON-IV system developed by Prof. Y. Noda of Tohoku University. The data collections were carried out in the (a^*, b^*) and (a^*, c^*) scattering planes. Lattice parameters were determined from the three reflections 400, 040 and 002: $a_0 = 7.63$Å, $b_0 = 13.30$Å and $c_0 = 9.64$Å at 250 K.

§3. Results

3.1 Diffraction data in the (a^*, b^*) planes

Figure 1 shows the temperature dependence of the integrated intensities of the 140 Bragg reflection and the $\frac{1}{2}\frac{9}{2}0$ superlattice reflection. The pressure variation on the process of cooling and

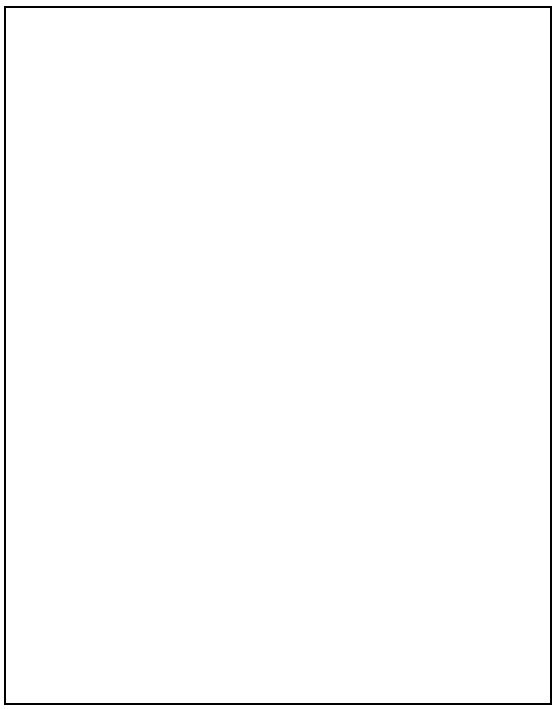

Fig. 1. The temperature dependence of the integrated intensities of the 140 Bragg reflection (circles) and the $\frac{1}{2}\frac{9}{2}0$ superlattice reflection (triangles). Full and open marks indicate on cooling and on heating, respectively. The temperature variation of the hydrostatic pressure is plotted by squares.

heating runs is also plotted. The superlattice reflections at the position of $\frac{h}{2}\frac{k}{2}\frac{l}{3}$: $h + k$=2n and

the Bragg reflections at the position $hk0$: $h+k=2n+1$ appeared at T_3 and T_4, respectively, in the low pressure region. Their intensity increased with decreasing temperature. At atmospheric pressure, phase IV is between T_3=112 K and T_4=76 K (see Fig. 1(a)).[8] As shown in Fig. 1(b), the transition temperature T_3 slightly increases with increasing pressure, while T_4 decreases rapidly with increasing pressure. The pressure coefficients of the transition temperatures are 7 K/kbar for T_3 and -45 K/kbar for T_4.

In Fig. 1(c), the 140 Bragg reflection appeared above about 80 K on heating or 60 K on cooling. Such Bragg reflections indicate that the commensurate phase with q_z=$\frac{1}{4}$ is stabilized at high pressure. The reflections with $h00$: $h=2n+1$ are systematically absent in this commensurate phase.

Figure 2 shows the relative magnitude of the observed structure factors; $|F(\pm h \pm k0)|/|F(hk0)|$: h =1 and k =3, and $h=\frac{1}{2}$ and $k=\frac{9}{2}$, at 80 K in phase IV. There was some scattering of data

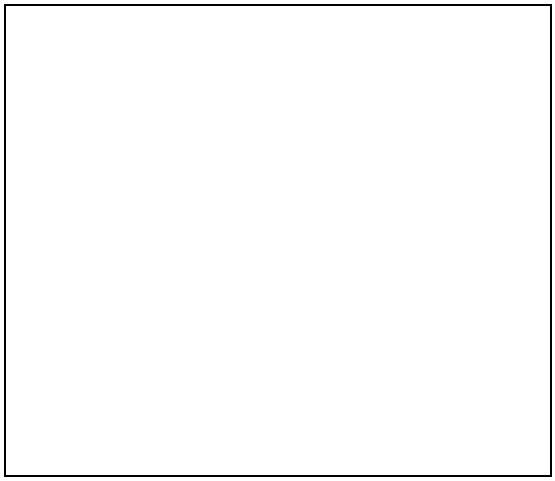

Fig. 2. The pressure dependence of the relative magnitude of observed structure factors: $|F(\pm h \pm k0)|/|F(hk0)|$; h =1 and k =3, and $h=\frac{1}{2}$ and $k=\frac{9}{2}$, at 80 K.

because of the difficulty of correction for absorption by ZrO_2 cylinder, Al_2O_3 cryostat-shroud and so on. No systematic relationship of these structure factors was detected in the 130, 220 and 330 Bragg reflections as well as the $\frac{1}{2}\frac{9}{2}$ 0 and $\frac{5}{2}\frac{3}{2}$ 0 superlattice reflections. Furthermore, the difference between the reflection condition in phase IV at atmospheric pressure and that under high pressure was not recognized.

The energy scan with constant Q at 0.45 0.55 0 at 70 K under pressure of about 0.7 kbar is shown in Fig. 3. Two soft modes, mode S and A, were observed, where these modes are defined in ref. 8.

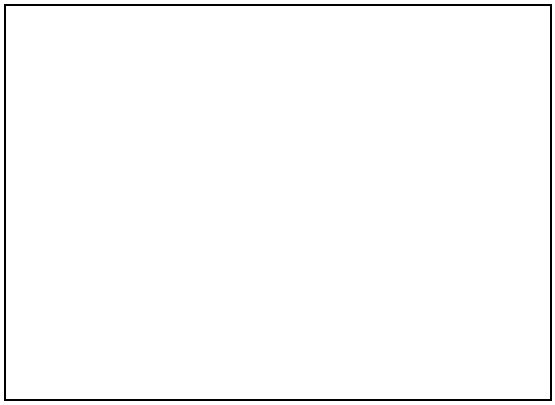

Fig. 3. Energy scan with constant Q at 0.45 0.55 0 at 70 K. The excitation peaks of the soft modes A ($\sim$ -0.3 meV) and S ($\sim$ -1.3 meV) are indicated by arrows.

The peak shape and the peak positions of the modes are similar to those at atmospheric pressure.

3.2 Diffraction data in the (a^*, c^*) planes

Figures 4, 5 and 6 show the temperature dependence of the integrated intensities of the $20\frac{2}{3}$, $20\frac{5}{7}$, $20\frac{8}{11}$ and $20\frac{11}{15}$ superlattice reflections. The diffraction profiles at some typical temperatures are also drown. The hydrostatic pressure varied as indicated during the cooling and heating runs. We first applied pressure at room temperature, then we performed the cooling run, which was followed by the heating run. Although we could recognized that the pressure changed reversibly between the cooling and the heating runs, the transition temperatures showed a thermal hysteresis of about 30 K during heating and cooling runs and some of runs were not reversible; the modulation wavenumber did not recovered at room temperature under high pressure.

The temperature dependence of the satellite positions at various pressure is shown in Fig. 7. The high pressure q_z=$\frac{2}{7}$ phase can be considered as a stable commensurate phase because the modulation wave vector is realized reversibly after cooling and heating. On the other hand, the high-order commensurate phases of $q_z \simeq \frac{3}{11}$ and $\frac{4}{15}$ appear either on cooling or heating. These two modulation wave vectors were not observed under pressure by K. Parlinski *et al.*[9] Therefore, we refer these phases as metastable ones.

At high enough pressure, the commensurate phase of q_z=$\frac{1}{4}$ is stabilized just as reported by K. Parlinski *et al.*[9] In this phase, we recognized a systematic absence of reflection as $h00$: $h = 2n+1$ and $00l$: $l = 2n+1$. Here we note that four reflection intensities $|F(\pm h0 \pm l)|$ did not change in phases IV within an experimental error.

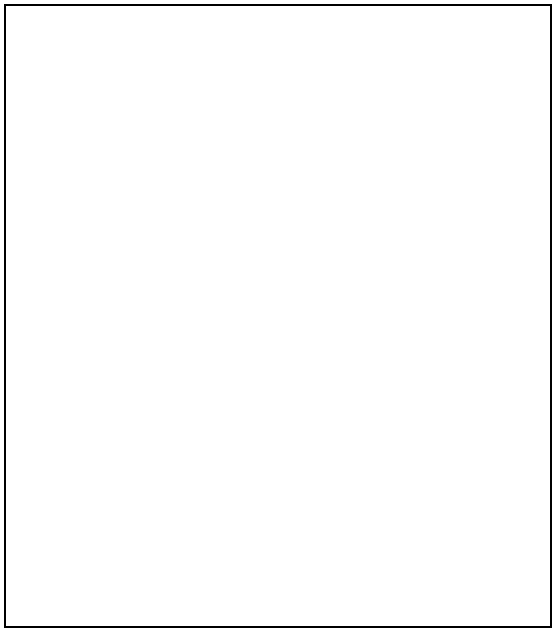

Fig. 4. The temperature dependence of the integrated intensities of the $20\frac{2}{3}$ and $20\frac{5}{7}$ superlattice reflections. Hydrostatic pressure is indicated by squares. The diffraction profiles at some typical temperatures are drawn in (b).

§4. Discussion

The effect of hydrostatic pressure on the phase transition at low temperature has been investigated by the use of neutron scattering technique. The pressure-temperature diagram can be summarized as shown in Fig. 8. We assign the transition temperatures as the middle point of the thermal hysteresis. The pressure coefficients of the transition temperatures are 7 K/kbar forT_3 and -45 K/kbar for T_4.

On the other hand, the pressure coefficient can be estimated by the use of the Ehrenfest relation for a second-order transition or the Clausius-Clapeyron relation for a first-order transition;[17)]

$$\frac{dT_3}{dp} = T_3 \frac{\Delta\beta}{\Delta C_p} \tag{4.1}$$

and

$$\frac{dT_4}{dp} = \frac{\Delta V/V}{\Delta S}, \tag{4.2}$$

where $\Delta\beta$ and ΔC_p stand for the discontinuity of the volume thermal expansion coefficient and the discontinuity in the specific heat, respectively, at the phase III-to-IV transition. $\Delta V/V$ and ΔS

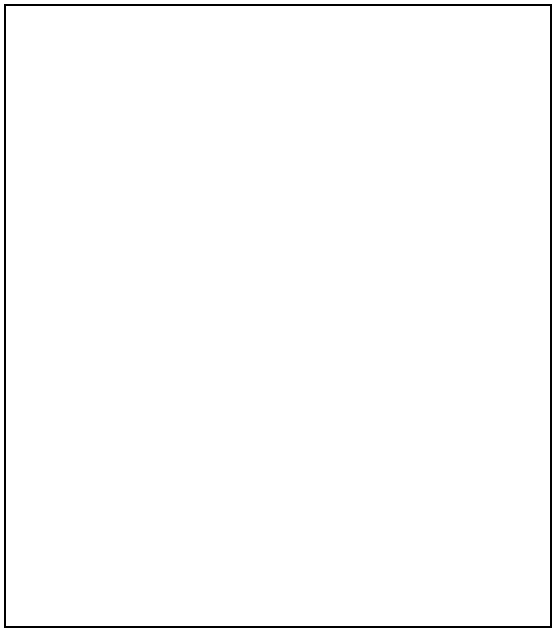

Fig. 5. The temperature dependence of the integrated intensities of the $20\frac{2}{3}$ and $20\frac{8}{11}$ superlattice reflections. The hydrostatic pressure is higher than that of Fig. 4. The diffraction profiles are drawn in (b) at various hydrostatic pressures.

stand for the discontinuity of the volume thermal expansion and the transition entropy, respectively, at the phase IV-to-V transition.

Using reported data[18,19] and the phase transition temperatures T_3=112 K and T_4=76 K, we can estimate the coefficients dT/dp are 8 K/kbar for T_3 and -147 K/kbar for T_4. The former value is in good agreement with our experimental value. The value is also comparable with those observed for the phase III-to-IV transition in K_2ZnCl_4 (6.8 K/kbar) and K_2CoCl_4 (8.4K/kbar).[20] On the other hand, the latter value is about three times larger than the experimental one. One of the reason for this discrepancy may be the large uncertainty involved in the used parameters for the calculation.

We observed no thermal hysteresis at the transition temperature between phase III and IV. The soft modes behaved to soften toward the transition point both from below and above T_3. It implies that this transition remains of second order even under hydrostatic pressure.

As for the commensurate q_z=$\frac{1}{4}$ phase which exits only under high pressure, three possible space groups, $Pc2_1n$, $P2_1/c11$ and $Pc11$, were proposed.[9] From the systematic absence of reflections, the space group of this commensurate phase is assigned to $P2_1/c11$.

To our disappointment, we could not control the pressure in the micro-cell within the cryostat;

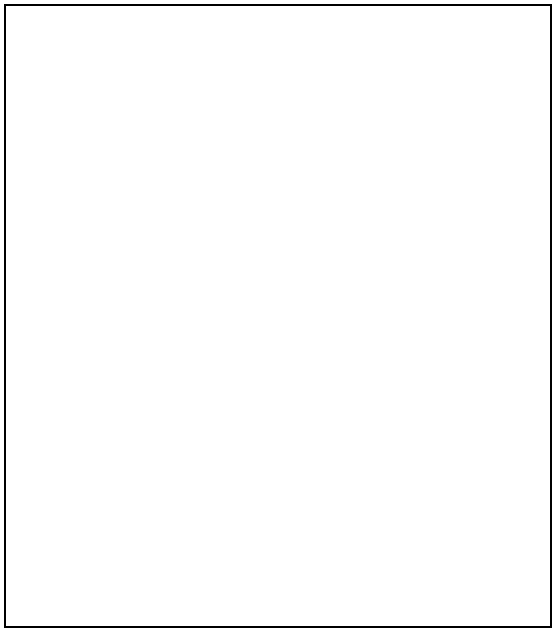

Fig. 6. The temperature dependence of the integrated intensities of the $20\frac{2}{3}$ and $20\frac{11}{15}$ superlattice reflections. The hydrostatic pressure is higher than that of Fig. 5. The diffraction profiles are drawn in (b) at various hydrostatic pressures.

the pressure varies with temperature. However, it was clearly demonstrated that the modulation wave vector locked-in values $q_z = \frac{2}{7}$, $\frac{3}{11}$ or $\frac{4}{15}$ under initial pressure at room temperature, and then the satellite position was pinned on cooling until the phase transition to the commensurate phase of $q_z = \frac{1}{3}$ took place. On heating, it seemed that the crystal transformed to the more stable commensurate phases of $q_z = \frac{2}{7}$ or $q_z = \frac{1}{4}$.

A good interpretation of these high pressure phases has been provided by the theory based on the extended axial next-nearest-neighbor Ising model[21] or the Chen-Walker model[22,23] for A_2BX_4-type crystals. It can be derived a similar rule that between two neighboring low-order commensurate phases of $q_z = \frac{n}{m}$ and $\frac{n'}{m'}$, the high-order commensurate phase appears with the modulation wave vector:

$$q_z = \frac{n+n'}{m+m'}. \tag{4.3}$$

It is remarkable that newly observed wave vectors of $q_z = \frac{3}{11}$ and $\frac{4}{15}$ are just the rational fractions given by eq. (4.3). If we represent the commensurate phase of $q_z = \frac{1}{3}$ by $\uparrow\downarrow\downarrow = < 21 >$ and that of $q_z = \frac{1}{4}$ by $\uparrow\uparrow\downarrow\downarrow = < 2 >$, then the commensurate phase of $q_z = \frac{2}{7}$ is written by $\uparrow\downarrow\downarrow\uparrow\uparrow\downarrow\downarrow = < 2^3 1 >$. In this notation, the high-order commensurate phases represented by $< 2^{2n+1}1 >$ with n=1, 2, and

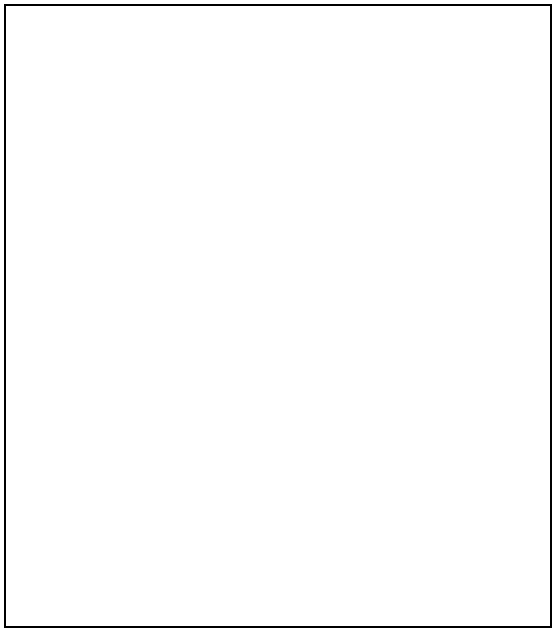

Fig. 7. The temperature dependence of the satellite positions at various pressure. Runs (a), (b) and (c) correspond to Fig. 4, Fig. 5 and Fig. 6, respectively.

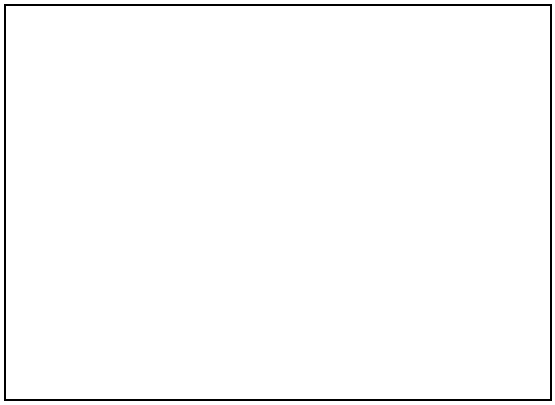

Fig. 8. Pressure-temperature phase diagram at low temperature of Rb_2ZnBr_4. Only the stable commensurate phases are represented. Full circles show the observed transition points. Dotted lines indicate the phase boundaries given in ref. 9.

3 were observed in our experiment. On the other hand, Parlinki *et al*[9] reported other sequence of high-order commensurate phases under pressure. The origin of the discrepancy is not dissolved.

Finally, it should be noted that the reflection condition did not seem to change, and the relative magnitude of the structure factors persisted to satisfy the *mmm* symmetry in phases III, IV and V, even at high pressure. Therefore, we could not definitely determine the structure of phase IV. In order to establish which model is actually the most appropriate representation of phase IV, it is necessary to collect scattering intensities very carefully, and to refine the crystal structure very accurately. The results of structural analysis for phase IV by the use of synchrotron radiation will be reported elsewhere.

Acknowledgments

One of the authors (H.S.) would like to thank Prof. T. Yamaguchi of Meisei University for fruitful discussions and providing me with the original data of thermal expansion in Rb_2ZnBr_4.

1) S. Sawada, Y. Shiroishi, A. Yamamoto, M. Takashige and M. Matsuo: J. Phys. Soc. Jpn. **43** (1977) 2101.
2) C. J. de Pater and C. van Dijk: Phys. Rev. **B18** (1978) 1281.
3) K. Gesi and M. Iizumi: J. Phys. Soc. Jpn. **45** (1978) 1777.
4) T. Ueda, S. Iida and H. Terauchi: J. Phys. Soc. Jpn. **51** (1982) 3953.
5) H. Kasano, H. Shigematsu, H. Mashiyama, Y. Iwata, H. Kasatani and H. Terauchi: J. Phys. Soc. Jpn. **63** (1994) 1681.
6) T. Yamaguchi and S. Sawada: J. Phys. Soc. Jpn. **60** (1991) 3162.
7) H. Shigematsu, H. Mashiyama, Y. Oohara and K. Ohshima: Physica **B 219&220** (1996) 611.
8) H. Shigematsu, H. Mashiyama, Y. Oohara and K. Ohshima: J. Phys. :Condensed Matter **10** (1998) 5861.
9) K. Parlinski, R. Currat, C. Vettier, I. P. Aleksandrova and G. Eckold: Phys. Rev. **B46** (1992) 106.
10) I. P. Aleksandrova, K. Parlinski, R. Currat, C. Vettier and G. Eckold: Ferroelectrics. **143** (1993) 17.
11) K. Gesi: Ferroelectrics **64** (1985) 97.
12) K. Gesi: Phase Transitions **40** (1992) 187.
13) I. P. Aleksandrova, E. V. Shemetov and V. L. Serebrennikov: Sov. Phys. Solid State **29** (1987) 1527.
14) I. P. Aleksandrova: in *Magnetic Resonance and Related Phenomena*, Poznan. (1988) 21.
15) A. V. Kityk, V. P. Soprunyuk and O. G. Vlokh: Phys. Solid State **35** (1993) 783.
16) A. Onodera, Y. Nakai, N. Kunitomi, O. A. Pringle, H. G. Smoth, R. M. Nicklow, R. M. Moon, F. Amita, N. Yamamoto, S. Kawano, N. Achiwa and Y. Endoh: Jpn. J. Appl. Phys. **26** (1987) 152.
17) M. Hebbache: Phys. Rev. **B44** (1991) 2796.
18) K. Nomoto, T. Atake, B. K. Chaudhuri and H. Chihara: J. Phys. Soc. Jpn. **52** (1983) 3475.
19) T. Yamaguchi and F. Shimizu: J. Korean Phys. Soc. **32** (1998) S244.
20) I. N. Flerov, T. Yamaguchi, S. Sawada, M. V. Gorev and K. S. Aleksandrov: J. Phys. Soc. Jpn. **61** (1992) 1606.
21) Y. Yamada and N. Hamaya: J. Phys. Soc. Jpn. **52** (1983) 3466.
22) Z. Y. Chen and M. B. Walker: Phys. Rev. Lett. **65**(1990) 1223.
23) Z. Y. Chen and M. B. Walker: Phys. Rev. **B43** (1991) 5634.

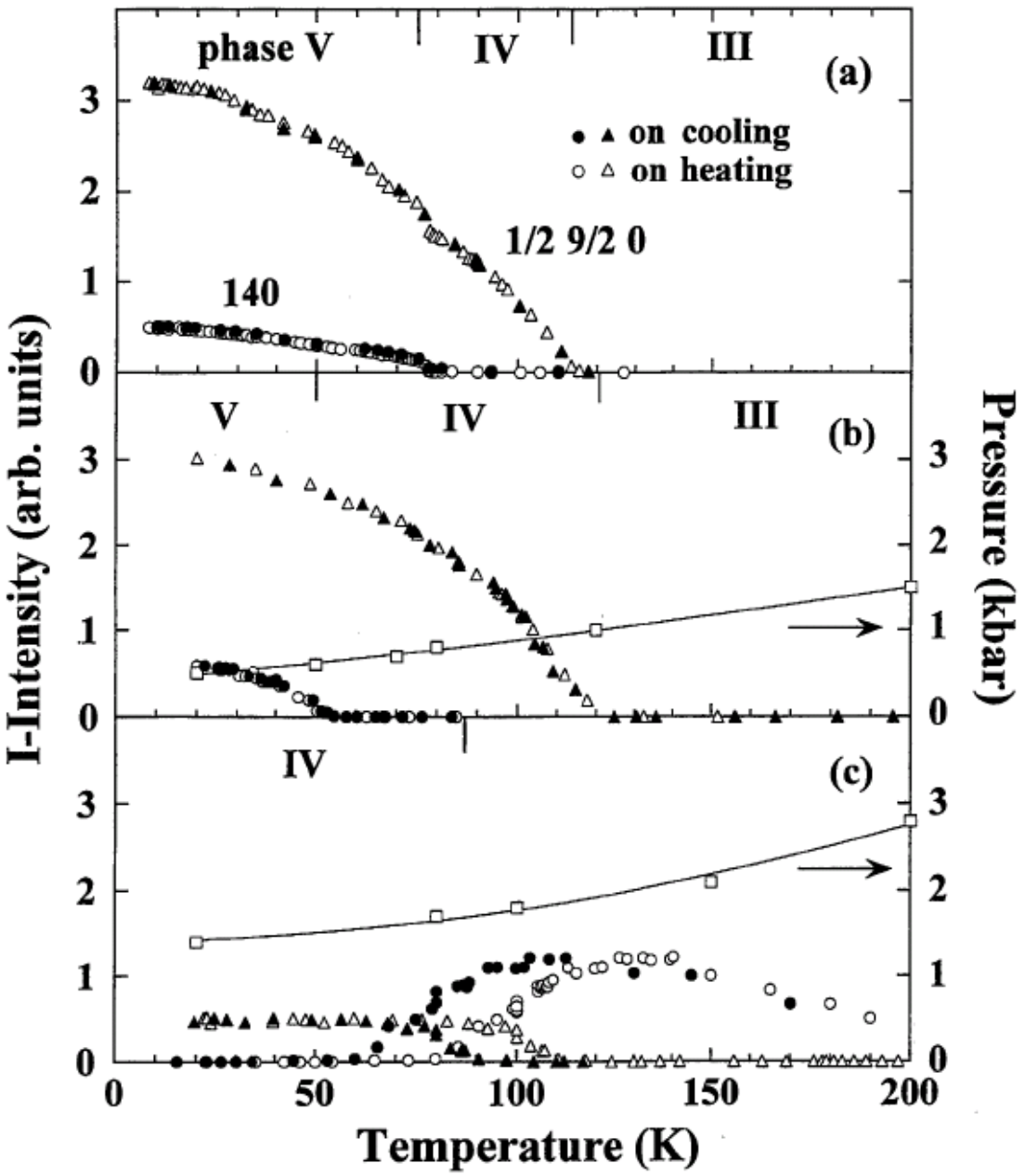
phase V
IV
III
(a)
on cooling
on heating
1/2 9/2 0
140
V
IV
III
(b)
IV
(c)
I-Intensity (arb. units)
Pressure (kbar)
Temperature (K)
0
50
100
150
200

Fig. 1.

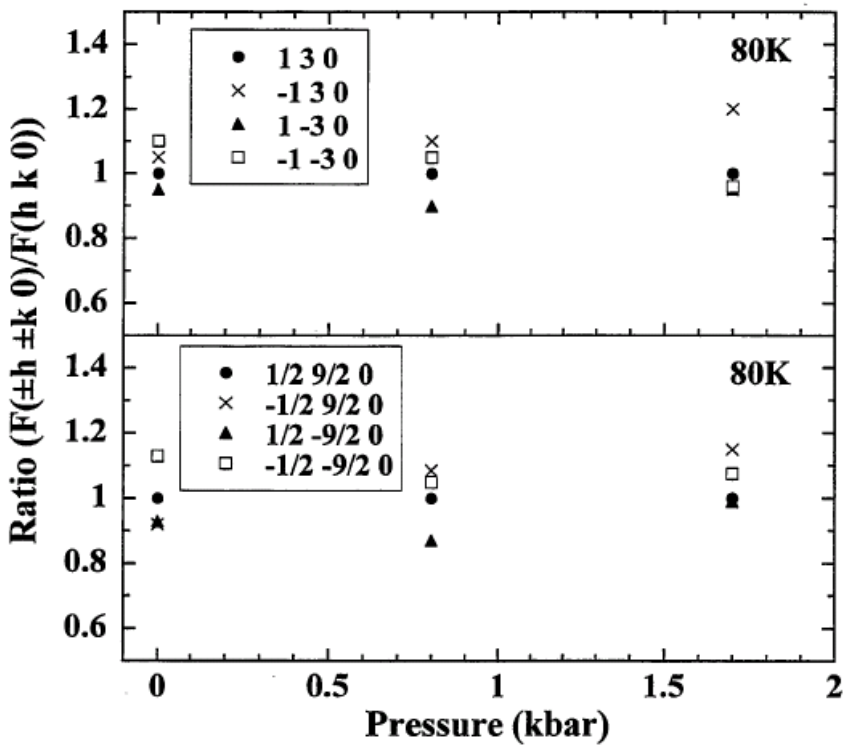
Ratio (F(±h ±k 0)/F(h k 0))
1.4
1.2
1
0.8
0.6
1 3 0
-1 3 0
1 -3 0
-1 -3 0
80K
1/2 9/2 0
-1/2 9/2 0
1/2 -9/2 0
-1/2 -9/2 0
80K
0
0.5
1
1.5
2
Pressure (kbar)

Fig. 2.

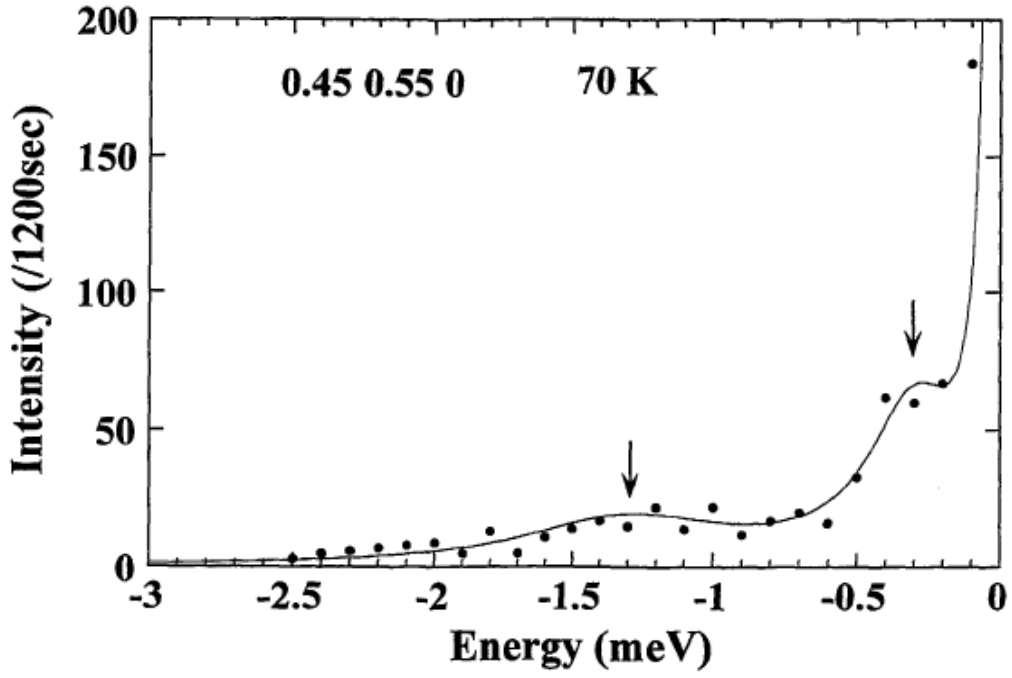
Intensity (/1200sec)
200
150
100
50
0
0.45 0.55 0
70 K
-3
-2.5
-2
-1.5
-1
-0.5
0
Energy (meV)

Fig. 3.

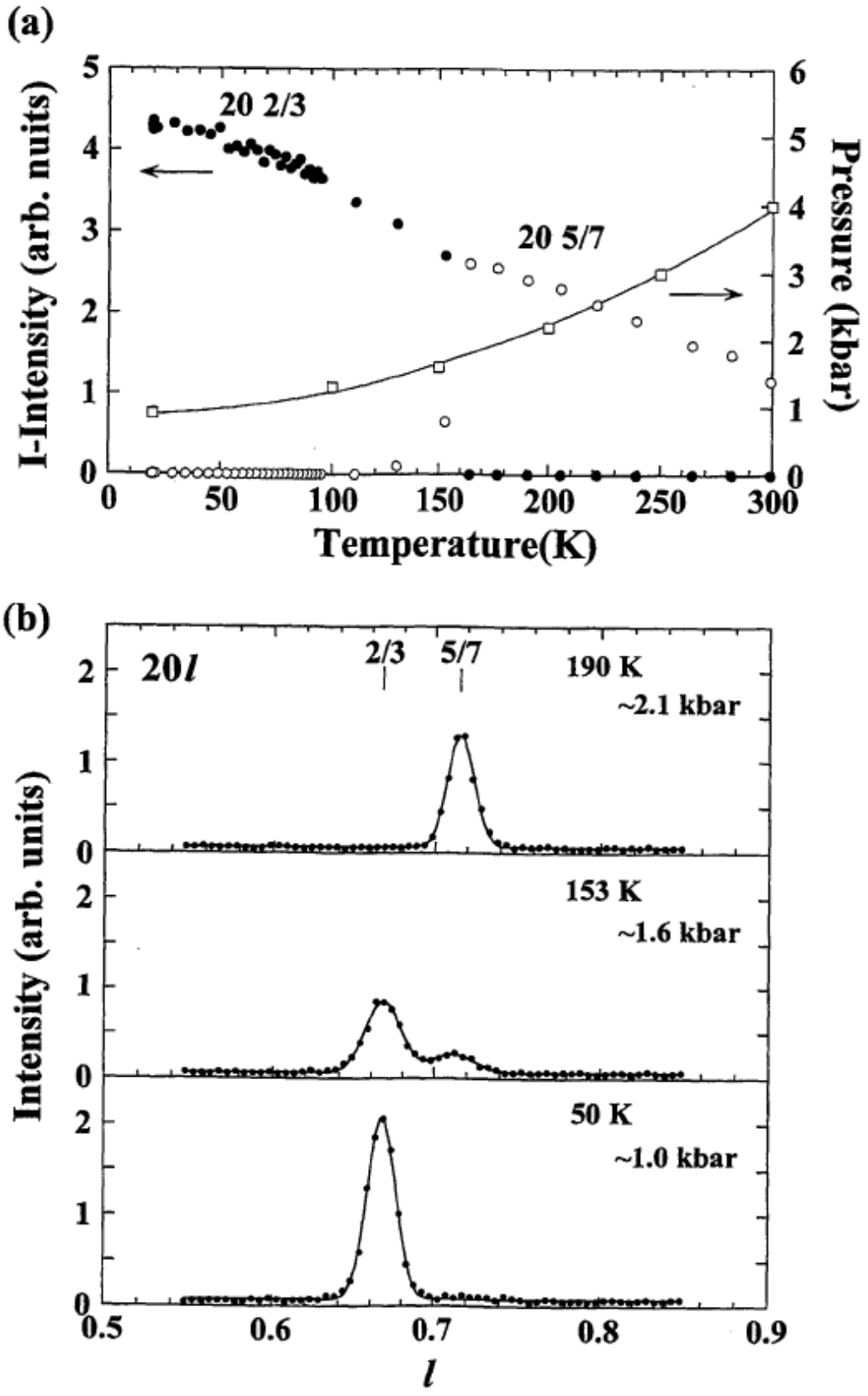
(a)
I-Intensity (arb. nuits)
Pressure (kbar)
20 2/3
20 5/7
Temperature(K)
(b)
Intensity (arb. units)
20l
2/3
5/7
190 K
~2.1 kbar
153 K
~1.6 kbar
50 K
~1.0 kbar
l

Fig. 4.

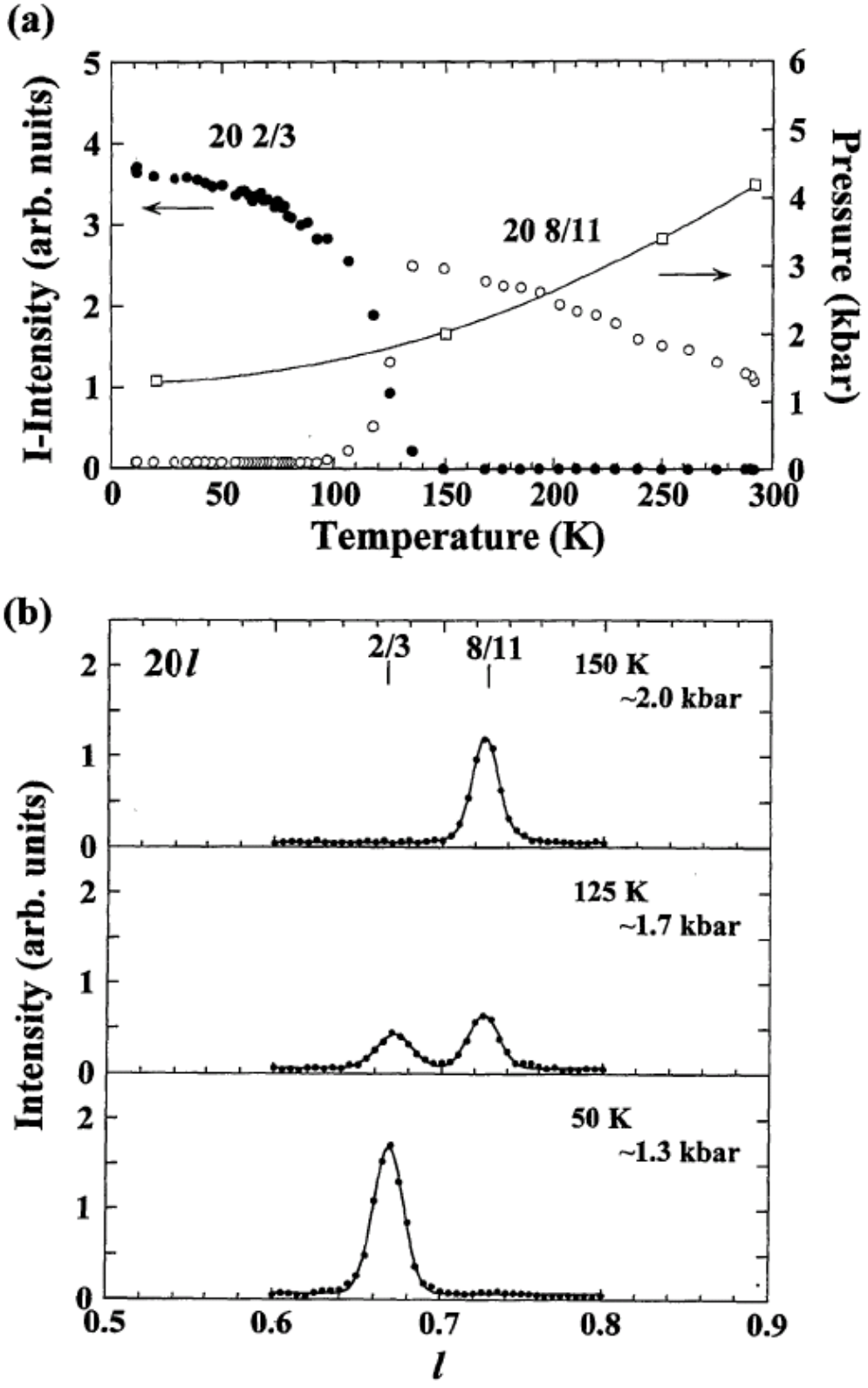
(a)
I-Intensity (arb. nuits)
Pressure (kbar)
20 2/3
20 8/11
Temperature (K)
(b)
Intensity (arb. units)
20l
2/3
8/11
150 K
~2.0 kbar
125 K
~1.7 kbar
50 K
~1.3 kbar
l

Fig. 5.

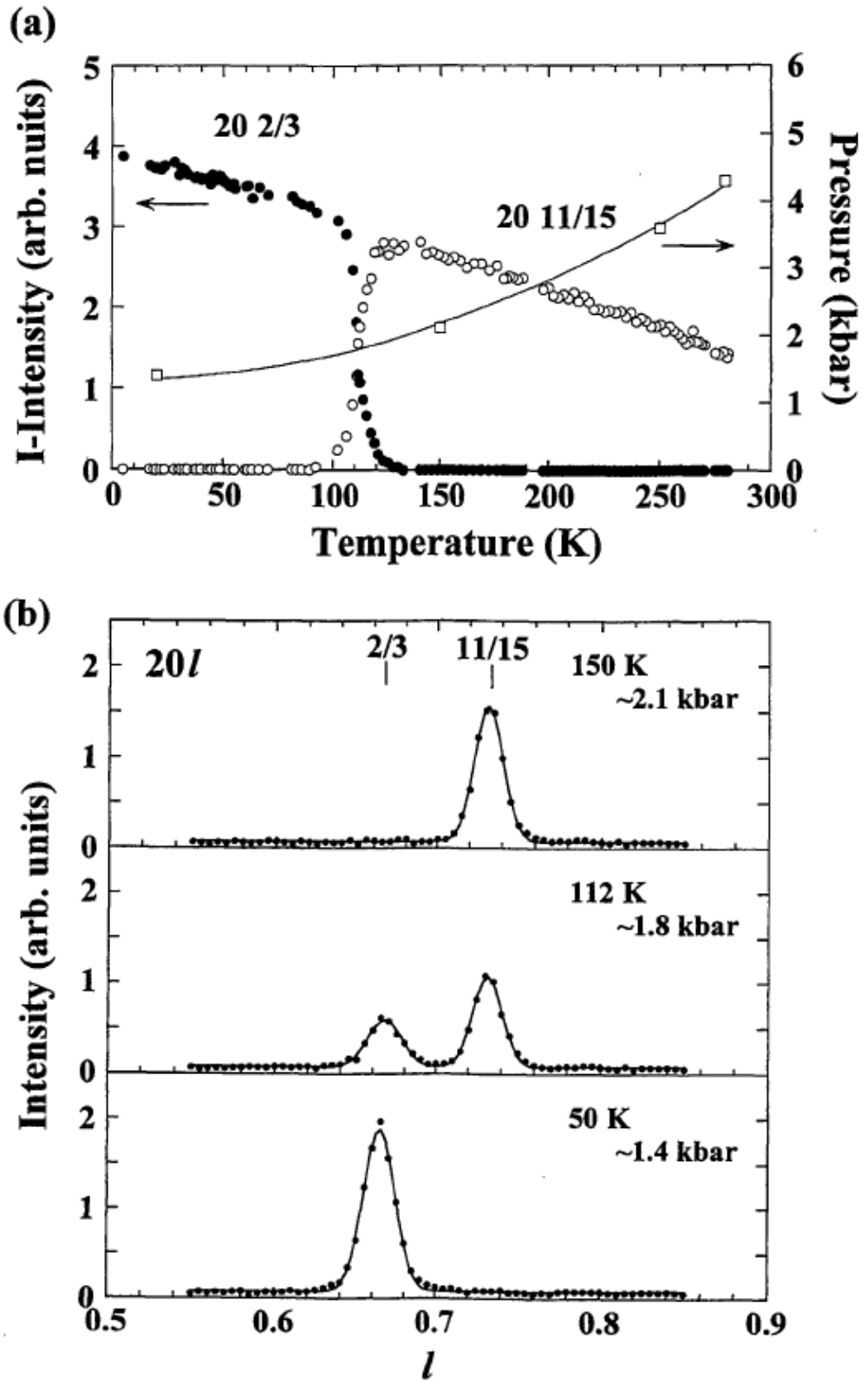
(a)
I-Intensity (arb. nuits)
Pressure (kbar)
20 2/3
20 11/15
Temperature (K)
(b)
Intensity (arb. units)
20l
2/3
11/15
150 K
~2.1 kbar
112 K
~1.8 kbar
50 K
~1.4 kbar
l

Fig. 6.

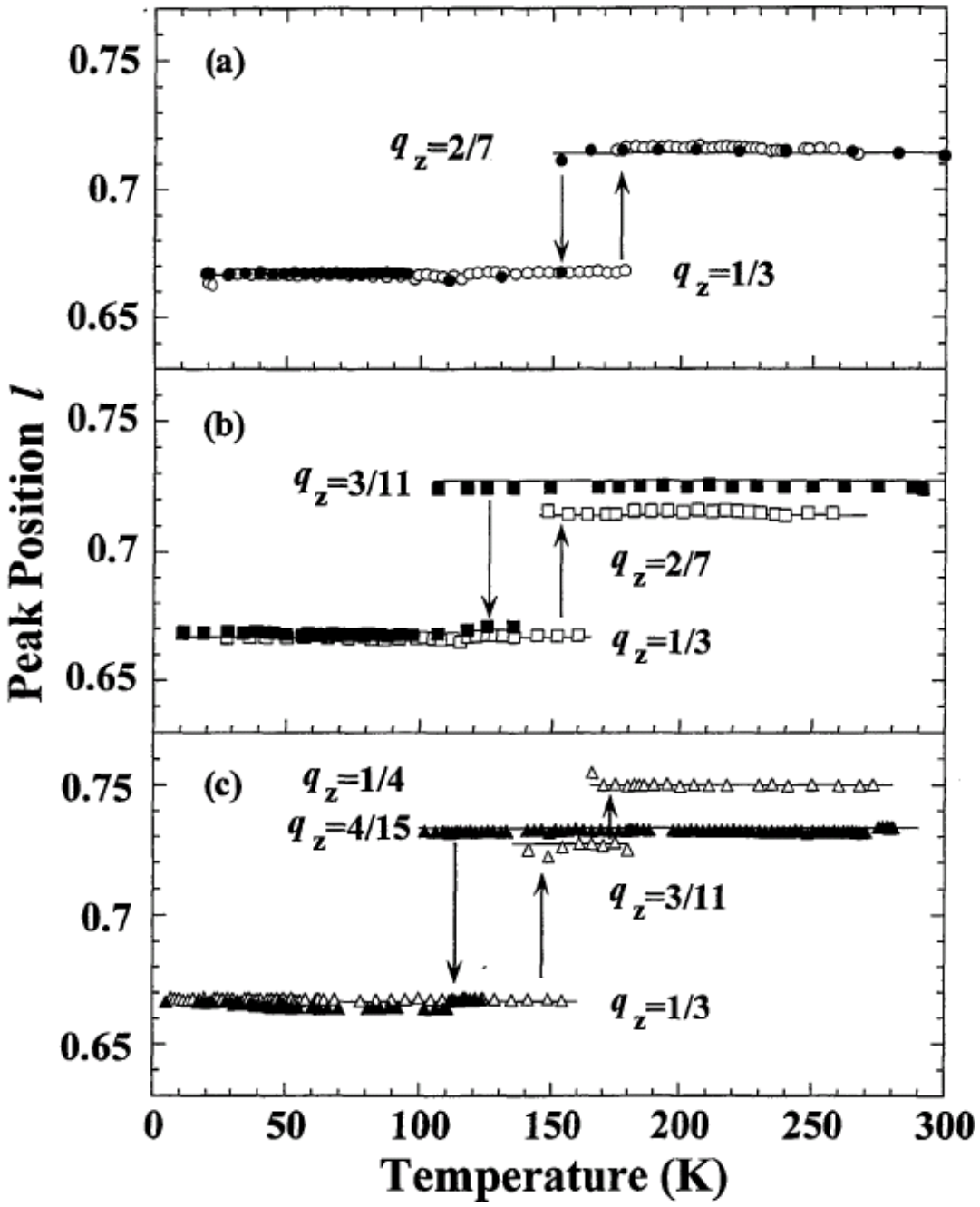
(a)
q_z=2/7
q_z=1/3
(b)
q_z=3/11
q_z=2/7
q_z=1/3
(c)
q_z=1/4
q_z=4/15
q_z=3/11
q_z=1/3
Peak Position l
0.75
0.7
0.65
0
50
100
150
200
250
300
Temperature (K)

Fig. 7.

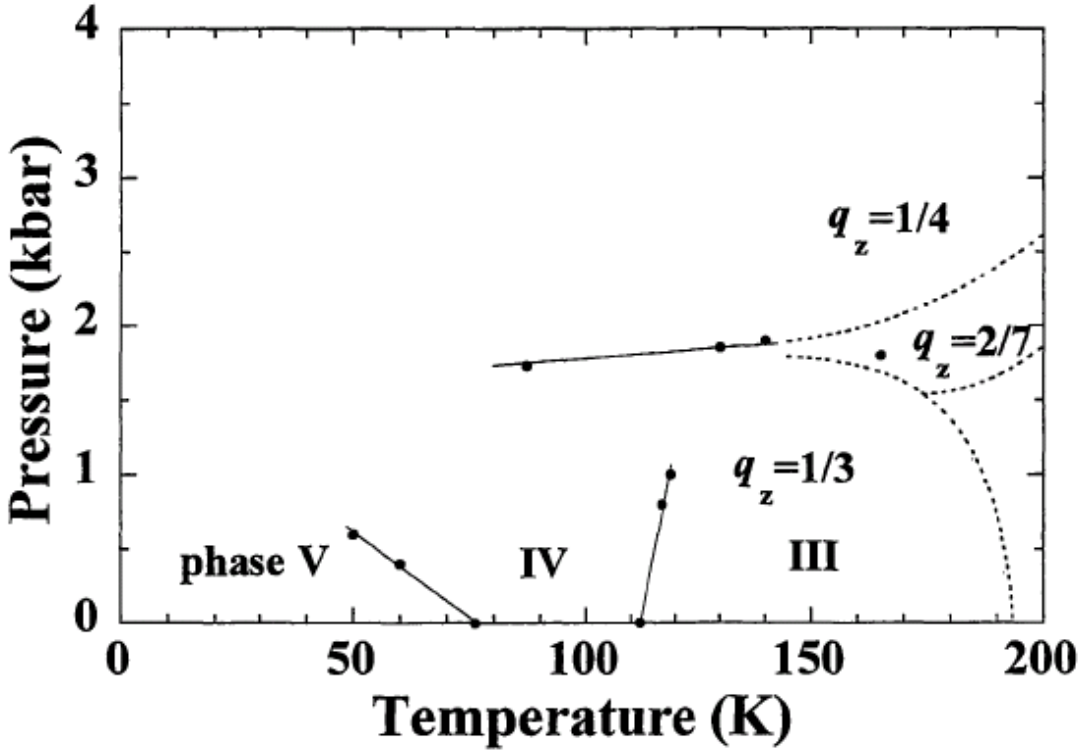
Pressure (kbar)
Temperature (K)
0
1
2
3
4
0
50
100
150
200
q_z=1/4
q_z=2/7
q_z=1/3
phase V
IV
III

Fig. 8.